Fossil coccolith morphological attributes as a new proxy for deep ocean carbonate chemistry

Authors: Amanda Gerotto[1,3]*, Hongrui Zhang[2]*, Renata Hanae Nagai[3], Heather M. Stoll[2], Rubens César Lopes Figueira[1], Chuanlian Liu[4], Iván Hernández-Almeida[2]

[1]Oceanographic Institute, University of São Paulo, São Paulo, Brazil; [2]Geological Institute, ETH Zurich, Zurich, Switzerland; [3]Center for Marine Studies, Federal University of Paraná, Pontal do Paraná, Brazil; [4]State Key Laboratory of Marine Geology, Tongji University, Shanghai, China.

*Corresponding authors: gerottoamanda@alumni.usp.br, zhh@ethz.ch

Abstract

Understanding the variations in past ocean carbonate chemistry is critical to elucidating the role of the oceans in balancing the global carbon cycle. The fossil shells from marine calcifiers present in the sedimentary record are widely applied as past ocean carbon cycle proxies. However, the interpretation of these records can be challenging due to the complex physiological and ecological response to the carbonate system during an organisms' life cycle, as well as the potential for preservation at the seafloor. Here we present a new dissolution proxy based on the morphological attributes of coccolithophores from the Noëlaerhabdaceae family (*Emiliania huxleyi* > 2 µm, and small *Gephyrocapsa* spp.). To evaluate the influences of coccolithophore calcification and coccolith preservation on fossil morphology, we measured morphological attributes, mass, length, thickness, and shape factor (ks) of coccoliths in a laboratory dissolution experiment and surface sediment samples from the South China Sea. The coccolith morphological data in surface sediments were also analyzed with environment settings, namely surface temperature, nutrients, pH, chlorophyll-a concentration, and carbonate saturation of bottom water by a redundancy analysis. Statistical analysis indicates that carbonate saturation of the deep ocean explains the highest proportion of variation in the morphological data instead of the environmental variables of the surface ocean. Moreover, the dissolution trajectory in the ks *vs*. length of coccoliths is comparable between natural samples and laboratory dissolution experiments, emphasizing the importance of carbonate saturation on fossil coccolith morphology. However, the mean ks alone cannot fully explain the main variations observed in our work. We propose that the normalized ks variation, which is the mean ks and standard deviation of ks (σ) over the mean ks (σ/ks), could reflect different degrees of dissolution and size-selective dissolution, influenced by the assemblage composition. By applying together with the σ/ks ratio, the ks factor of fossil coccoliths in deep ocean sediments could be a potential proxy for a quantitative reconstruction of past carbonate dissolution dynamics.

1. Introduction

The ocean's large reservoir capacity of carbon dioxide (CO_2) plays an essential role in the carbon cycle and, consequently, in controlling atmospheric CO_2 (Ridgwell and Zeebe, 2005; Wang et al., 2016). The ocean CO_2 is influenced by temperature, salinity, and biological activity, including primary production, respiration, calcification, and carbonate dissolution (Ridgwell and Zeebe, 2005; Sarmiento and Gruber, 2006; Libes, 2009; Wang et al., 2016). When CO_2 dissolves in water, the ocean becomes more acidic, decreasing pH, carbonate ion concentration, and carbonate saturation (Ω_{Ca}). The carbonate compensation depth (CCD) is the depth at which the rate of calcite dissolution is balanced by the rate of calcite supply. The CCD is usually several hundred meters deeper than the chemical lysocline, the saturation horizon of calcite, due to the kinetics of dissolution (Ridgwell and Zeebe, 2005). Whereas the photic zone is supersaturated with respect to calcite in most areas of the ocean, large areas of the deep ocean are currently undersaturated because of the increased solubility of calcite with pressure (Sulpis et al., 2018). As the ocean continues absorbing larger amounts of CO_2 from anthropogenic fuel emissions, a shallowing of the CCD is expected for the next 100 years due to the sharp decrease of carbonate saturation from surface to deep ocean (Hönisch et al., 2012; USGCRP, 2017; Sulpis et al., 2018; IPCC, 2019). Variations in the CCD on timescales from millions to several thousands of years are an important process in determining the ocean's carbonate chemistry and regulating atmospheric CO_2 (Emerson and Archer, 1990; Pälike et al., 2006). Understanding the role of physical and biogeochemical parameters in marine carbonates is therefore critical to interpret the geological record correctly and to reconstruct variations in the ocean carbon cycle in the past.

The effects of carbonate chemistry changes and variations in the position of the CCD in the geological past have been investigated using a wide array of geochemical and microfossil proxies such as $\delta^{13}C$ in benthic and planktonic foraminifera (Zachos et al., 2005; Hönisch et al., 2012), fragmentation indices of calcareous microfossils (Le and Shackleton, 1992; Broerse et al., 2000; Flores et al., 2003), and $CaCO_3$ content (Archer et al., 2000; Palike et al., 2006) in marine sediments. However, these proxies do not provide quantitative estimates of past changes in carbonate chemistry because some additional ecological mechanisms determine the calcification and preservation responses (Hönisch et al., 2012; Rae et al., 2021). $\delta^{11}B$ provides a quantitative proxy for past seawater pH (Hönisch et al., 2012), albeit additional carbonate chemistry parameters impose some limits on the interpretation of the proxy (Yu and Elderfield, 2007; Rae et al., 2021). Benthic B/Ca provides a quantitative proxy for deep sea CO_3^{-2} concentration (Yu et al., 2016). Yet both of these methods require mono-specific foraminifera

samples for measurements, which are time-consuming to pick, and analyses are limited to sediment samples that contain sufficient concentration of this microfossil group.

Coccolithophores, a group of single-celled calcifying algae, are characterized by the production of calcite plates called coccoliths. Coccoliths are the main constituent of marine biogenic sediments, contributing up to 80 % of deep-sea carbonate fluxes (Young and Ziveri, 2000; Hay, 2004). Changes in coccoliths morphology, distribution, and abundances are believed to record the evolution history of coccolithophores and reflect the environmental conditions in the surface ocean (i.e., during coccolith biomineralization) (Riebesell et al., 2000; Iglesias-Rodriguez et al., 2008; Beaufort et al., 2011; Charalampopoulou et al., 2016; Rigual-Hernández et al., 2020a). Because of that, coccoliths are widely used in paleoclimate and paleoceanographic reconstructions (e.g., Bollman and Herrle, 2007; Rickaby et al., 2007; Henderiks and Pagani, 2007; Bolton et al., 2016). Several methods exist to estimate coccolithophore calcification in the fossil record. Assumed proportional length and thickness allowed for the first estimates of coccolith mass using microscope techniques (Young and Ziveri, 2000). More recent methods based on the optical properties of calcite under polarized light microscopy (circular and linear) allowed a more precise estimate of the thickness of individual coccoliths (Beaufort, 2005; Bollman et al., 2014; Fuertes et al., 2014; Johnsen and Bollmann, 2020; Beaufort et al., 2021). The optical techniques have been successfully employed in downcore records to estimate coccolithophore calcification across time and evolutionary steps (e.g., Bolton et al., 2016; Beaufort et al., 2022; Guitián et al., 2022). However, until now there has been no study that evaluates the response of calcification patterns of fossil coccolithophores to both environmental parameters controlling biomineralization in the photic zone and calcite saturation state at the depth of burial.

The South China Sea (SCS) is the largest marginal basin of the Western Pacific, characterized by very dynamic spatial environmental conditions and a steep bathymetric profile (Wang et al., 2015). Sediment records from this basin have been used to study the response of coccolithophores to different environmental variables. Previous studies found positive correlations between coccolithophore biometry from plankton samples and nutrients and light at the photic zone (Jin et al., 2016). Building on these results, but applied to the sedimentary record, Su et al. (2020) explored the dependency of coccolithophore weight and past surface ocean carbon chemistry parameters and nutrient conditions. However, it has also been demonstrated that there is intense coccolithophore dissolution above the lysocline in the SCS (Fernando et al., 2007a). More recently, a study using plankton tow material found that the degree of calcification in the coccolithophore species *Emiliania huxleyi* was insensitive to carbonate chemistry in surface waters (Jin et al., 2022a). This diversity of results calls for new

studies that systematically explore the drivers of coccolithophore morphology and calcification in the fossil record.

Here, we analyzed morphological attributes of fossil coccolithophores in surface sediment samples in the SCS, located across spatial environmental gradients in the surface ocean, but also across a bathymetric transect related to the calcite saturation at the seafloor which leads to lower calcite saturation at the seafloor in deeper sites. In addition, we evaluated the morphological variations of coccoliths under different dissolution intensities in a laboratory experiment. Using an automated algorithm to estimate coccolithophore calcification from images taken with a microscope under cross-polarization, we show that scale-invariant measures of coccolith thickness (shape factor, ks) from coccolithophores located along a depth gradient in the SCS are highly correlated to the calcite saturation state at the seafloor. We propose a new calibration to reconstruct past calcite saturation based on ks which would enable the quantitative reconstruction of changes in the calcite saturation in the deep ocean and position of the CCD in the past.

2. Oceanographic settings

The SCS is a marginal basin located in the Western Pacific, connected to the open ocean by shallow passages to the north and south (Fig. 1A). The Luzon Strait in the north is the deepest (~2000 m) and the principal channel for water exchange between the SCS and the Pacific through the Kuroshio Current (Qu et al., 2006; Liu et al., 2011; Wan and Jian, 2014). The modern surface circulation and hydrographic characteristics of the SCS are directly associated with the seasonal changes promoted by the East Asian Monsoon (EAM; Wang and Li, 2009). These seasonal hydrodynamic patterns control the regional sea surface temperature (SST) distribution, salinity, and nutrients (Fig. 1B-E, Wang and Li, 2009). The SST latitudinal gradient is up to 2° C with an annual average of 28-29° C in the southern SCS and 26-27° C in the north (Tian et al., 2010). Salinity varies seasonally between 32.8-34.2 psu, with smaller salinity variation in the north than in the south (Wang and Li, 2009). Northern SCS primary productivity reflects the seasonality of the EAM with more productive and well-mixed waters during the winter season (Zhang et al., 2016), with higher chlorophyll-*a* concentration (0.65 mg Chl-α m^{-3} and 600 mg C m^{-2} d^{-1}) (Chen, 2005; Chen et al., 2006; Jin et al., 2016).

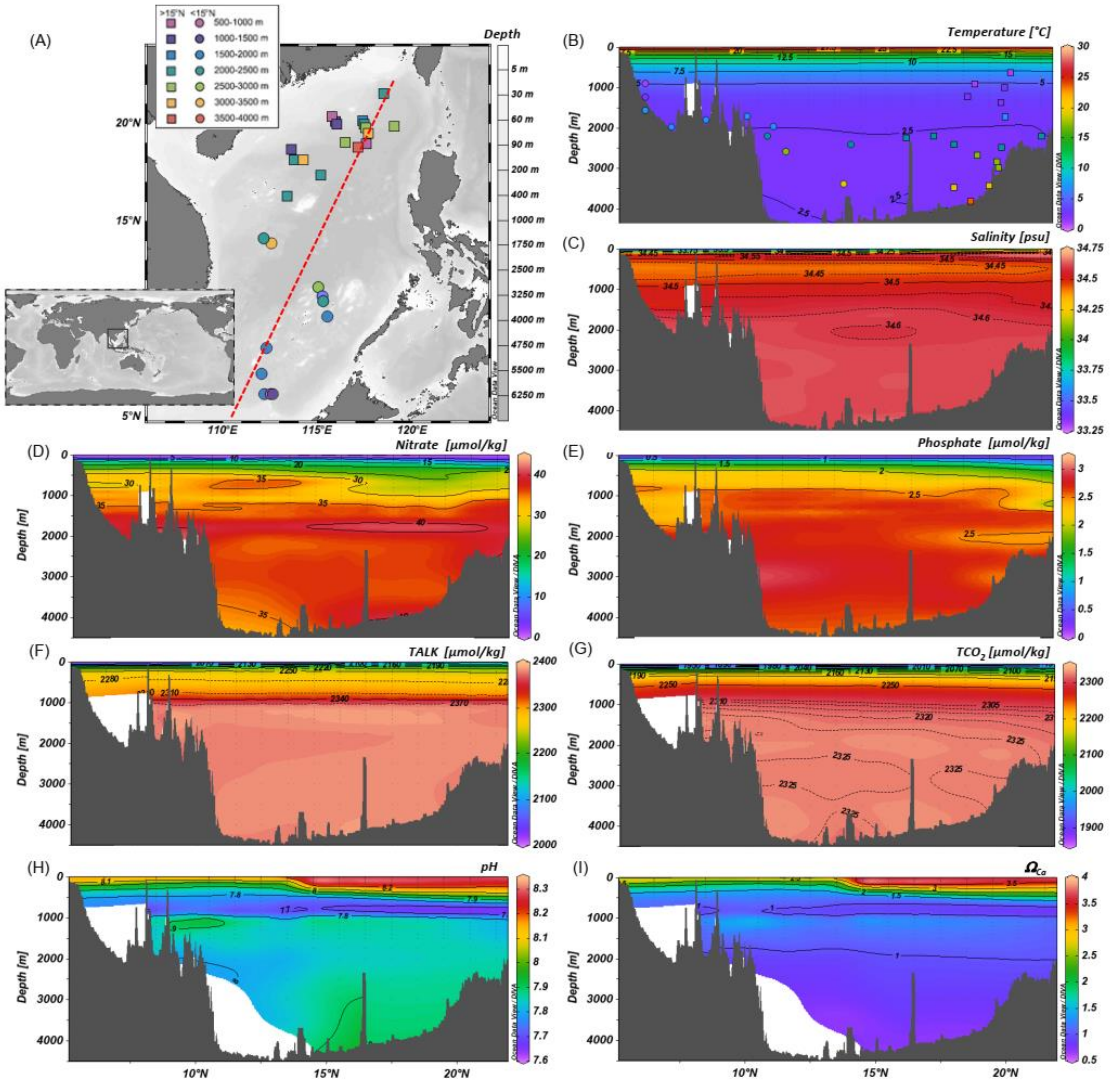

Figure 1. Map of the South China Sea and location of core-top samples used in the present study. Dots and squares represent stations located from 6° to 15° N, and from 15° to 22° N. (A). Vertical profiles along N-S (5° to 22° N) transect (dotted red line on panel A) of (B) temperature, (C) salinity, (D) nitrate, and (E) phosphate, (F) total alkalinity (TALK) and (G) total inorganic carbon concentration (TCO_2), (H) pH and (I) Ω_{Ca} calculated at CO2SYS (Pierrot et al., 2012). See M&M 3.3 section for data sources. The map and the vertical profiles were plotted with Ocean Data View (ODV) software (Schlitzer, 2019). Colored dots in panel (B) indicate the geographical position along the transect shown in panel (A) of the surface sediment samples used in this study.

The modern SCS lysocline is approximately 1200 m, and the CCD lies between 3500 and 3800 m (Thunell et al., 1992; Wang et al., 1995; Luo et al., 2018). In the northern SCS, surface waters (e.g., the upper 300 m) are characterized by relatively low DIC and TALK (Fig. 1F-G) and

higher pH and Ω_{Ca}, compared to deeper waters (Fig. 1H-I) (Chou et al., 2007; Jin et al., 2016). Below 1000 m, the SCS across a N-S transect is characterized by relatively homogeneous DIC, $\delta^{13}C$, and [CO_3^{2-}] (Chen et al., 2006; Qu et al., 2006; Chou et al., 2007; Wan et al., 2020).

The SCS deep waters originate from the North Pacific Deep Water (NPDW) that penetrates the marginal basin through the Luzon Strait (Qu et al., 2006; Liu et al., 2011; Wan and Jian, 2014; Wan et al., 2018). The route traced from the Luzon Strait to the northwest suggests a predominantly cyclonic deep circulation (Qu et al., 2006; Wang and Li, 2009). The deep-water residence time of the SCS is estimated to be approximately 30-50 years, like that of intermediate waters, 52 years (Chen et al., 2001). Due to this short residence time, the SCS presents a homogeneous vertical profile; below 2000 m, there are no evident chemical stratification or changes compared to the Pacific deep-water chemistry (> 2000 m) characteristics (Chen et al., 2001; 2006; Qu et al., 2009). The rapid residence time potentially implies that, when replaced, deep waters occupy intermediate water levels (between 300 m and 1300 m), contributing to the circulation of intermediate and shallow waters and ocean-atmosphere exchanges (Qu et al., 2009; Tian et al., 2010).

3. Material and methods

3.1 Material and sample treatments

The core-top samples (n =28) employed in this study were retrieved from different depths in the basin of SCS (Fig. 1) during the R/V Sonne cruises (SO-95) (Table 1). Toothpick samples from each location were used to prepare smear slides, without any chemical or physical treatment, following standard micropaleontological procedures (Marsaglia et al., 2015). Unfortunately, the surface sediments were already depleted resulting in not having enough material to perform dissolution experiments using the same samples. For the dissolution experiment, we employed 240 mg of dry sediment obtained from a Late Pleistocene sample from the Western Equatorial Pacific (Ocean Drilling Program -ODP- 807A-2H-2W, 57-59 cm). The distribution of coccolithophore species belonging to the Noëlaerhabdaceae family in the sample ODP 807 is 41% of *G. oceanica*, 34% of *G. caribbeanica* and 23% of small *Gephyrocapsa*. These taxa are thicker particularly *G. caribbeanica,* than the thinner Noëlaerhabdaceae species commonly found in the SCS (e.g., *E. huxleyi,* Roth and Berger, 1975; Roth and Coulbourn, 1982). The sediment sample was suspended in 120 ml Milli-Q water, and then the suspension was separated into 6 centrifuge tubes, each with a volume of 20 mL and containing the equivalent of 40 mg of sediment. Sodium hexametaphosphate $(NaPO_3)_6$ (Calgon®) has traditionally been used in pretreatment of samples with calcareous microfossils, particularly foraminifera (Olson and Smart 2004; Smart et al., 2008). However, it has been observed that application of this

chemical agent dissolves these microfossils due to complexation of Ca with phosphates, an effect which varies with the exposure time (Feldmeijer et al., 2013). Therefore, we added 100 mg of Calgon® into 100 ml Milli-Q water, resulting in a concentration of 1.6mM, to conduct our dissolution experiment. Different volumes of Calgon® solution (0, 0.4, 0.8, 2, 4 6 ml) were added to each of the six subsamples. The Calgon® is very corrosive to the fine carbonate particles, and the reaction between Calgon® and carbonate could be simplified in two steps. First, the $(NaPO_3)_6$ hydrolysis releases the sodium trimetaphosphate ($Na_3P_3O_9$). Then, the calcium in the solution is exchanged with sodium and precipitate as $Ca(PO_3)_2$, $CaNa(PO_3)_3$, and $CaNa_4(PO_3)_6$, strongly reducing the free calcium concentration in the solution. The decrease in calcium concentration promotes carbonate dissolution. In theory, adding 1 mol $(NaPO_3)_6$ would result in the dissolution of 3 mol $CaCO_3$ at maximum. So, there could be ~80 % carbonate left even after adding 6 ml Calgon® solution. The particles in all tubes were kept suspended gently by a rotating disaggregation wheel as described previously (Stoll and Ziveri, 2002) for two days to achieve a full reaction between carbonate and $(NaPO_3)_6$. Slides were prepared for coccolith morphological analyses using the drop technique as described by Bordiga et al. (2015) to trace the variations of coccolith amount during dissolution.

3.2 Coccolith morphological parameters

The morphological parameters of coccoliths in the dissolution experiment and surface sediment were analyzed using a Polarized Microscope (Zeiss Axio Scope HAL100), configured with circularly polarized light and a Zeiss Plan-APOCHROMAT 100x/1.4 oil objective, and a coupled camera (Zeiss Axiocam 506 Color). For every sample, at least 40 fields of view were photographed. After species identification and selection of coccolithophores images belonging to the Noëlaerhabdaceae family (*Emiliania huxleyi* > 2 µm, and small *Gephyrocapsa* spp.), each sample had between 100 and 400 (average of 250 per sample) coccolithophore images. The relationship between the color of coccolith images and thickness was calibrated using a reference calcite wedge, the thickness of which had been carefully quantified (González-Lemos et al., 2018). After calibration, all images were analyzed in the Matlab-based software, C-Calcita (Fuertes et al., 2014), to obtain the coccolith morphological parameters, including length, volume, and mass. The length-shape factor of each coccolith, ks, was calculated using the formula by Young and Ziveri (2000) based on the coccolith mass and length obtained from C-Calcita:

$$\mathrm{ks} = \frac{Mass}{2.7 \times Length^3}$$

Beyond the traditional morphological parameters, we calculated the normalized ks variation, which is the ratio of the standard deviation of ks (σ) over the mean ks (σ/ks). The goal of this novel parameter is to provide a new dimension to trace the dissolution process in coccoliths, especially when the coccolith assemblage is diverse. For example, if the coccoliths dissolve at different speeds in the assemblage due to differential sensitivity to acidification, a small increase of σ/ks would be expected at the beginning of the dissolution because of the σ increase and ks decrease. Then, after all fragile coccoliths dissolve, leaving only thicker coccoliths in the assemblage, the σ/ks should show a decreasing trend which could be mainly caused by a decrease σ.

Table 1. Station, coordinate data, and water depth of core-top samples used in this study.

Station	Longitude (E)	Latitude (N)	Water depth (m)
17930	115.782	20.333	629
17965	112.552	6.157	889
17943	117.553	18.95	917
17931	115.963	20.1	1005
17944	113.637	18.658	1219
17963	112.667	6.167	1233
17932	116.037	19.952	1365
17964	112.213	6.158	1556
17960	115.558	10.12	1707
17940	117.383	20.117	1728
17961	112.332	8.507	1795
17959	115.287	11.138	1957
17962	112.082	7.182	1970
17949	115.167	17.348	2195
17957	115.31	10.9	2197
17941	118.483	21.517	2201
17951	113.41	16.288	2340
17945	113.777	18.127	2404
17955	112.177	14.122	2404
17939	117.455	19.97	2473
17958	115.082	11.622	2581
17934	116.462	19.032	2665

17938	117.538	19.787	2835
17925	119.047	19.853	2980
17956	112.588	13.848	3387
17937	117.665	19.5	3428
17946	114.25	18.125	3465
17936	117.12	18.767	3809

3.3 Environmental data for surface sediment

Annual means of different physical, chemical and biological variables in both 50 m depth and bottom water for the location of the surface samples (Table 1) were extracted from different databases, interpolated to the geographical location of the surface sediment samples. Here the 50 m depth was selected because it is the depth at which the highest concentration of Noëlaerhabdaceae coccolithophorid is observed in the SCS (Jin et al., 2016). Seawater temperature, salinity, nitrate, and phosphate concentrations (used as a proxy of phytoplankton) at 50 m were obtained from WOA01 (Fig. 1B,C,D,E). Sea surface chlorophyll-a concentration data were based on MODIS data (2003-2016) extracted from Oregon State University Ocean Productivity (http://www.science.oregonstate.edu/ocean.productivity/). Annual averaged concentrations of total alkalinity (TALK) and dissolved inorganic carbon (TCO_2) were extracted from Goyet et al. (2000) (Fig. 1F,G). Then the carbonate ion concentration, ph (Fig. 1H), pCO_2 for the depth of 50 m and Ω_{Ca} for the seafloor depth were calculated by CO2SYS macro for Excel® (Pierrot et al., 2012) (Fig. 1I) using salinity, temperature, pressure, total phosphate, total silicate, TALK, and TCO_2 at the corresponding depth (50 m or depth of the surface sediment sample). The light intensity at 50 m water depth was calculated using a model of penetration of photosynthetic active radiation (PAR) from surface to depth (Buiteveld, 1995; Murtugudde et al., 2002), monthly climatologies of PAR from the MODIS Ocean database (http://oceancolor.gsfc.nasa.gov/cgi/l3), and the diffuse attenuation coefficient for downwelling irradiance at 490 nm (Kd490) and Equation 1 in Lin et al. (2016).

3.4 Statistical analysis

Pearson correlation and redundancy analysis (RDA) were employed to explore the relationship between morphological features of the coccoliths in surface sediment samples and the environmental data. All statistical analyses were performed using the PAST 4.06 software (Hammer et al., 2001).

4. Results

4.1 Variations of coccoliths morphology in the dissolution experiment

In the dissolution experiment, mean ks decreased with increasing volume of Calgon® solution (Fig. 2A). The mean ks varied between 0.12 (0 ml Calgon®) and 0.04 (6 ml Calgon®) (Fig. 2A). The σ/ks represents variation in preservation among coccoliths within each sample. Higher differences in σ were observed in samples containing 2 ml, 4 ml, 0.8 ml, 0.4 ml, 0 ml, and 6 ml, respectively (Fig. 2B). Increasing the amount of Calgon® solution up to 2 ml showed a decrease in mean ks and an increase in σ. Samples with 4 and 6 ml Calgon® solution showed a reduction in mean ks and σ among coccoliths (Fig. 2B). The lowest mean ks (0.04) and the maximum mean length (3.95 µm) were recorded under the higher Calgon® solution (6 ml) amount (Fig. 2C). Increased amounts of Calgon® solution also resulted in a gradual increase in coccolith length leading to a negative correlation between length and ks (r= -0.68, $p > 0.05$), but not significant due to the small number of observations (Fig. 2C).

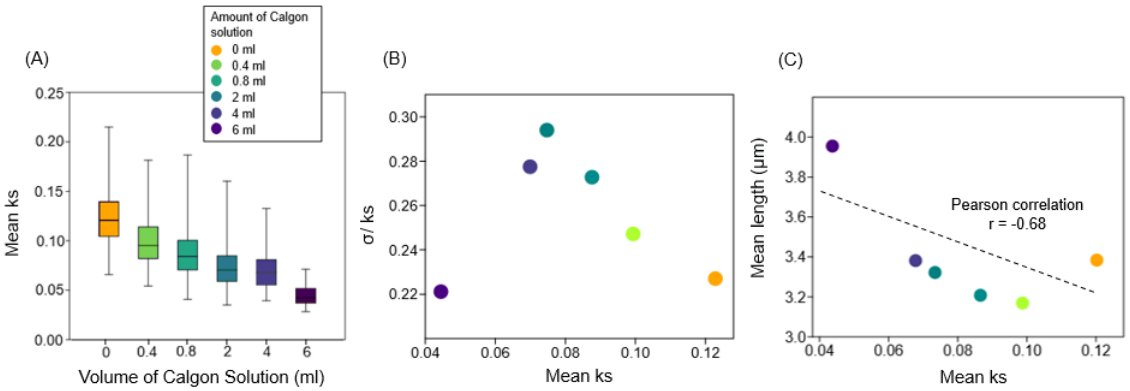

Figure 2. Coccolith morphological variations in the dissolution experiment. (A) Box plots of the median (horizontal line inside the boxes), minimal and maximal values of coccoliths mean ks (vertical bars) under the different volumes of Calgon® solution; (B) Scatter plot of mean ks and σ/ks and (C) linear correlation and correlation coefficient ($p > 0.05$) between mean ks and mean length.

4.2 Variations in coccolith morphology in natural conditions

Overall, the mean ks, thickness, and volume in the core-top sampling stations (Fig. 3) presented higher values in shallower depths. The mean ks varied between 0.03 and 0.07, and the mean thickness was between 0.25 and 0.44 µm, with maximum values recorded at station 17931 located in northern SCS at 1005 m water depth. The mean length of coccolith varied between 3.23 and 3.78 µm, with the highest values recorded at 2195 m water depth (site 17949) in northern SCS, but without a significant trend along depths. The mean volume of coccoliths ranged between 1.70 and 2.97 μm^3, and the mean mass was between 4.61 and 8.03 pg, with

maximum values for both recorded in the shallowest station (e.g., 17930), at 629 m water depth in northern SCS.

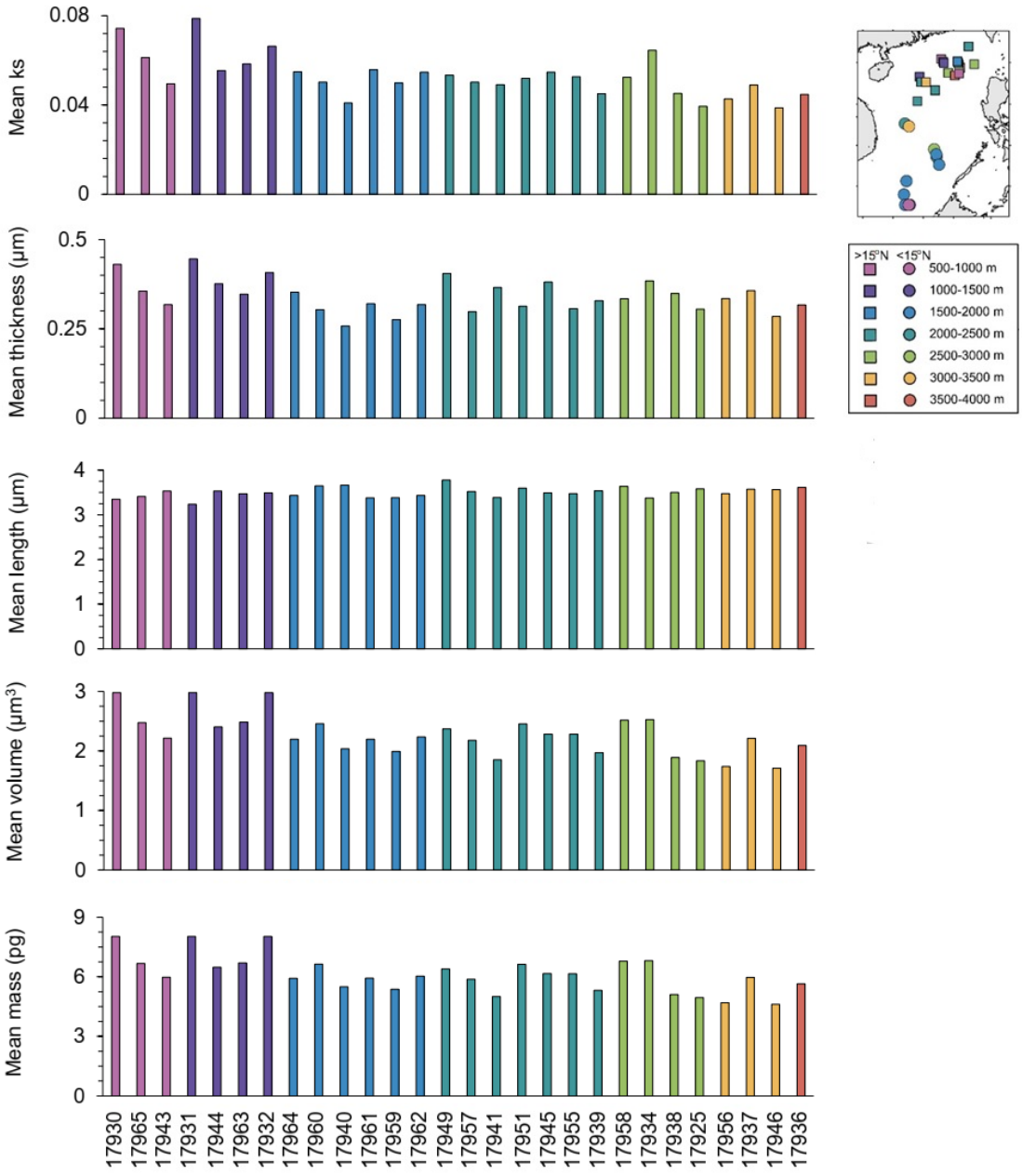

Figure 3. Coccolith mean ks, thickness (µm), length (µm), volume (µm^3), and mass (pg) in surface samples from SCS. The sampling stations are distributed along the x-axis according to their depth, sorted from the shallowest to the deepest.

In general, the degree of dissolution varied according to the depth of the sediment samples. The calcite saturation, Ω_{Ca}, decreases with colder temperature, higher pressure and higher CO_2 concentration in deep ocean. The normalized ks variation presents different trajectories associated with light, strong, or no dissolution (Fig. 4A). The shallowest stations

south (<15˚ N) and north SCS (> 15˚ N) show a linear and increasing trend between ks and σ/ks. For the samples below 2000 m, there is no clear pattern of variation related to the mean ks standard deviation. However, samples below 3000 m are mainly located on the left upper part of the plot, in a similar position as the samples treated with 4 and 6 ml of Calgon® in the normalized ks variation comparison of the dissolution experiment (Fig. 3B). The mean ks *vs*. mean length shows a negative correlation ($r = -0.62$, $p < 0.05$), with the deepest samples showing larger size coccoliths and lower mean ks (Fig. 4B).

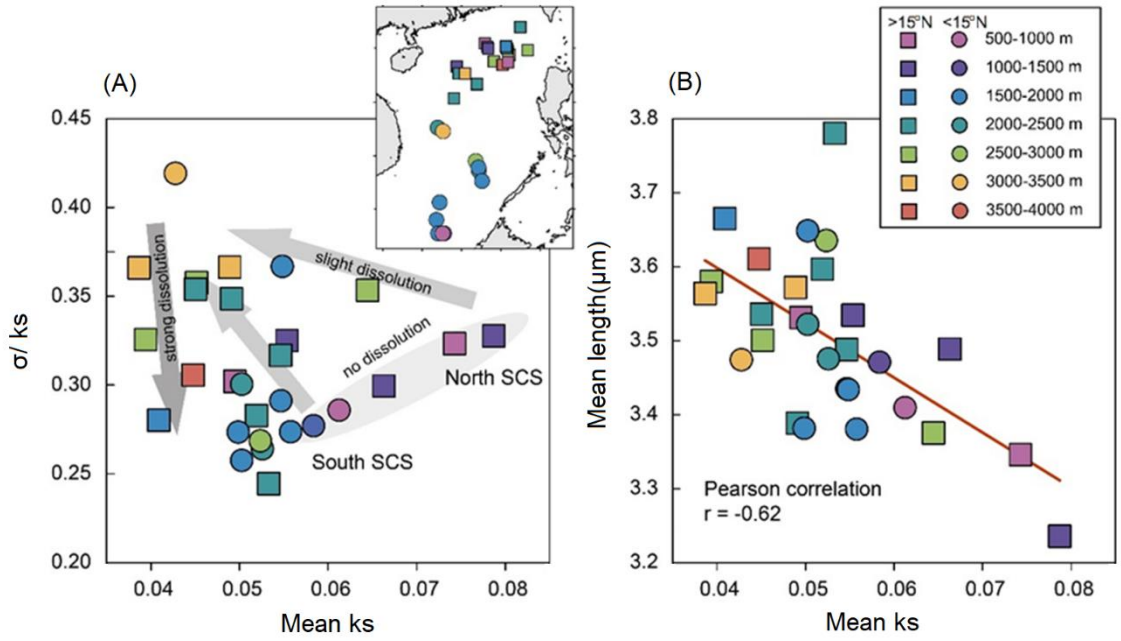

Figure 4. Morphological parameters of coccolith in surface sediments (A) Scatter plot between mean ks and σ/ks and (B) linear correlation and correlation coefficient ($p < 0.05$) between mean ks and mean length. Shaded arrows in panel A represent ideal trajectories of the normalized ks variation (mean ks *vs.* σ/ks) as shown in figure 2B, to interpret the trends in the surface sediment samples. Note that the mean ks of figures 2 and 4 are different due to the higher abundance of the species *G. caribbeanica,* with higher thickness, in the sample for the dissolution experiment.

We analyzed the correlations between the biological and environmental datasets (Table 2). Although some of the surface variables were autocorrelated (e. g., TALK-salinity, pH-pCO_2 and nitrate-phosphate), they were included in our analyses because some studies have identified a strong influence of these parameters on coccolith morphology during the life-cycle (e.g., Chen et al., 2007; Jin et al., 2016). Significant correlations can be found ($p < 0.05$) between several morphological parameters of coccolith and bottom water carbonate chemistry (Ω_{Ca}), with a correlation coefficient (r) = 0.67 between mean ks and Ω_{Ca}, r = 0.66 between mean volume and $\Omega_{Ca,}$ and r = 0.66 between mass and $\Omega_{Ca.}$ The mean thickness of the coccolith shows a

significant correlation with Ω_{Ca} at the sample depth (r = 0.41), and with the concentrations of nutrients nitrate and phosphate at 50 m (r = 0.44 and 0.4, respectively). Surprisingly, the mean length showed no significant correlation to any environmental variables except with PAR (r = 0.35).

The results of RDA can provide another critical perspective on the control of environmental variables on coccolith morphology. The RDA1 and RDA2 explain together 58.3 % of the total variations in coccolith morphological data. The surface sediment samples, color-coded by different depth intervals, are distributed along the axis of RDA1, which is the most important and explains 54.6 % of the total variance (Fig. 5A). Among the environmental variables, Ω_{Ca} shows the highest correlation to RDA1 (r = -0.67, $p < 0.05$). The results of both the correlation analyses and the RDA show that Ω_{Ca} in bottom water is the most important environmental variable driving the morphological dataset, which shows a high correlation with mean ks (r= 0.69; $p < 0.05$) and could explain up to 47 % (R^2= 0.47) of the variance observed in mean ks (Fig. 5B). The RDA2 explained 3.69 % of the variance and is mainly correlated to the salinity, temperature, pH, phosphate, TALK, and pCO_2 (Fig. 5A). The null response of coccolith length to any environmental parameter is also observed in the RDA plot by its position near the center of the ordination space, significantly contrasting with other morphological parameters (Fig. 5A).

Table 2. Correlation matrix (p-value and Pearson correlation) between biological and environmental variables. Bold values indicate significant correlations (with $p < 0.05$).

Environmental/ Biological	p value					r				
	Mean ks	Mean thickness	Mean length	Mean volume	Mean mass	Mean ks	Mean thickness	Mean length	Mean volume	Mean mass
Salinity	0.79	0.07	0.87	0.86	0.86	-0.05	0.34	0.03	-0.03	-0.03
Temperature	0.94	0,04	1.0	0.90	0.90	-0.01	-0.39	0.00	-0.02	-0.02
Phosphate	0.88	0.03	0.63	0.96	0.96	0.03	**0.41**	-0.09	-0.01	-0.01
Nitrate	0.36	0.02	0.30	0.71	0.71	0.17	**0.44**	-0.20	0.07	0.07
TALK	0.53	0.13	0.70	0.60	0.60	-0.12	0.28	0.07	-0.10	-0.10
Chlorophyll-a	0.26	0.18	0.88	0.18	0.18	0.22	0.25	-0.02	0.26	0.26
PAR	0.28	0.05	0.06	0.50	0.50	-0.21	-0.38	0.35	-0.13	-0.13
pH	0.18	0.31	0.38	0.24	0.24	-0.26	0.19	0.17	-0.22	-0.22
pCO_2	0.16	0.33	0.38	0.21	0.21	0.27	-0.19	-0.17	0.24	0.24
Ω_{Ca}	**0.00**	**0.03**	0.05	**0.00**	**0.00**	**0.67**	**0.41**	-0.36	**0.66**	**0.66**

TALK = total alkalinity, PAR = photosynthetic active radiation and, Ω_{Ca} = carbonate saturation.

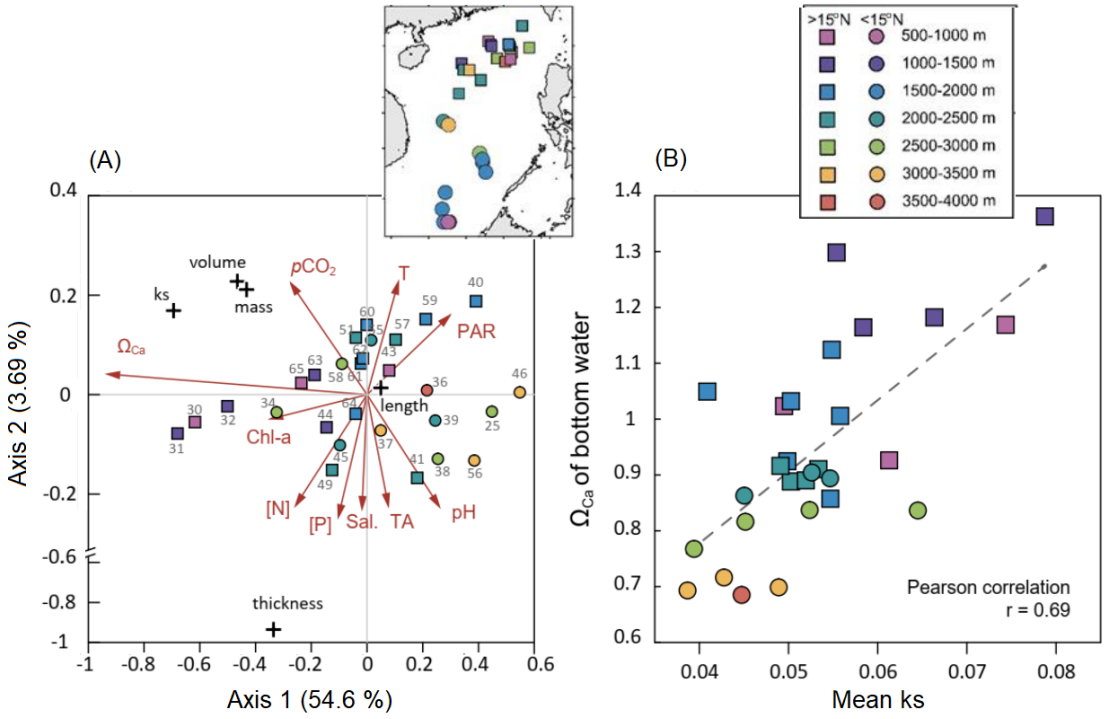

Figure 5. Redundancy analysis (RDA) ordinations for environmental variables and morphological measurements (A) and (B) linear correlation and correlation coefficient ($p < 0.05$) between Ω_{Ca} at bottom depths and mean ks from surface samples.

5. Discussion

5.1 Comparison between laboratory dissolution experiment and natural samples

In this study, we evaluate fossil coccolith responses to dissolution under laboratory experiments and field settings. In the dissolution experiment, ks values are higher than the modern coccoliths in the SCS due to the higher abundance of the relatively thicker *G. caribbeanica* in the downcore sediment sample. Though the absolute values of ks cannot be directly compared between the dissolution experiment (Fig. 2B) and surface sediments (Fig. 4A), the trajectory of morphological variations during the dissolution experiment does provide important diagnostic information to explain phenomena observed in the surface sediment samples.

First, the phenomenon that coccolith length increased with the decrease of ks could be observed in both the dissolution experiment (Fig. 2C) and natural surface sediments (Fig. 4B). The laboratory experiment showed that under controlled conditions (known changes in water chemistry and uniform species composition), the coccolith morphology variations (mean length

and mean ks) reflected different degrees of dissolution. We also observed a length-related dissolution pattern, where smaller coccoliths gradually dissolve with the increase in Calgon® concentration, leading to a higher average length but a lower mean ks. The mean ks and mean length relationships in the surface samples (Fig. 4B) show a similar trend to the laboratory observations (Fig. 2C). Thus, the observed trend and the largest size and lowest ks in the surface sediment samples are explained by the dissolution of the smallest species due to the lower Ω_{Ca} at the deepest samples and increasing the abundance of the larger coccoliths.

Second, changes in the σ/ks ratio in the dissolution experiment reflect a slight and gradual increase in dissolution and then a decrease with the highest concentrations of Calgon® (Fig. 2C). In the laboratory experiment, the subsample with no Calgon® solution presented well-preserved coccoliths with high mean ks and a small standard deviation. As the amount of Calgon® solution added to each subsample increases, small coccoliths start dissolving preferentially, decreasing the mean ks and increasing the standard deviation (Fig. 2B). With higher amounts of Calgon® solution (4 and 6 ml), the small coccoliths are completely dissolved, resulting in an assemblage dominated by larger coccoliths (Fig. 2C). Under these highest dissolution stages, the larger coccoliths are also partially dissolved then both mean ks and σ decrease (Fig. 2B). In this way, the σ reflects how differential dissolution size selection affects the composition of the assemblages. Hence, samples that are more (less) susceptible to dissolution result in more homogeneous (heterogeneous) assemblages regarding carbonate preservation.

However, the trajectory of the normalized ks variation in surface sediments seems more complex than in the dissolution experiment (Fig. 4A). First, there is a group of samples with a positive correlation between σ/ks and ks from shallow areas of the north and south SCS. The depth of samples from northern and southern SCS regions is similar, so we argue that this feature is not caused by dissolution but due to the assemblage composition differences in both parts of the SCS. The coccolithophores have multi-stage blooms in the north SCS, with a peak of *G. oceanica* in late winter, when coccolithophore fluxes are highest due to strong water column mixing and renewed nutrient inventory, and another of *E. huxleyi* in early spring (Chen et al., 2007; Jin et al., 2019). In contrast, *E. huxleyi* is the dominant species in the more oligotrophic south SCS (Fernando et al., 2007b) due to its higher competitiveness in situations of lower nutrient concentration (particularly nitrate) compared to *G. oceanica* (Eppley et al., 1969; Rhodes et al., 1995). So, even without any influence from dissolution, the assemblages in the north SCS should feature a higher species diversity and, thereby, a higher σ/ks compared with the coccolith in the south SCS. Hence, the variety of the coccolith assemblages in the surface sediment samples results in different trajectories in the normalized ks variation plotting.

But the general trend of the normalized ks variation in surface sediment is still following the trends observed in the dissolution experiment: (1) ks decreases with dissolution; (2) σ/ks increases slightly when dissolution starts and (3) then it decreases with greater dissolution.

5.2 Sedimentary record of coccolith morphology: calcification *vs*. dissolution factors

Previous studies have evaluated changes in the calcification of Noëlaerhabdaceae coccoliths in glacial-interglacial cycles through analyses of the coccolith mass and attributed morphological variations mainly to water column nutrient availability and carbonate chemistry parameters, related to the coccolithophores physiological response (e.g., Beaufort et al., 2011). Su et al. (2020) found that the environmental dynamics of the surface photic zone controlled Noëlaerhabdaceae coccoliths' calcification in northern SCS (MD05-2904). Similarly, higher calcite production recorded by increased coccolith mass has been attributed to the increased [CO_3^{2-}] in the surface water column in the South Indian Ocean and North Atlantic Ocean in modern sediments (Beaufort et al., 2011). Dissolution effects were thought to be less likely drivers of changes in the morphology of coccolith (Beaufort et al., 2011; Su et al., 2020), which is a reasonable assumption for the coccoliths depositing in shallow sediments above the lysocline. These interpretations are partially sustained by the findings of Beaufort et al. (2007), who found no significant coccolith dissolution during the settling in sediment traps deployed between 250 and 2500 m. The former study proposed that most of the dissolution occurs in the euphotic zone and possibly in the guts of grazers, therefore, discarding the impact of bottom water chemistry and/or post-burial processes on coccolithophore weight.

In our set of samples in the SCS, the RDA results show that mean thickness and length significantly correlate to nitrate and phosphate at 50 m (Table 2). This observation agrees with Jin et al. (2016), who found that biometric attributes of *E. huxleyi* correlated with nutrient concentrations in the plankton samples in the East China Sea (ECS). Nutrient variables are important for coccolithophore calcification (Raven and Crawfurd, 2012) and morphological parameters, at least in species of the Noëlaerhabdaceae family (Båtvik et al., 1997; Pasche et al., 1998). However, based on the extended evidence of our study, including carbonate chemistry at the depth of the sediment samples in the SCS, we observe evidence that several of the morphological parameters measured are not only influenced by primary biomineralization. Still, abiogenic post- or syn-depositional processes override this signal in the sediment samples in this region. The highest correlations between coccolith morphology, namely mean ks, volume, and thickness, with the bottom water calcite saturation, Ω_{Ca}, indicates that the calcium carbonate preservation conditions could strongly override some of the morphological parameters in fossil

coccoliths (Table 2, Fig. 5A). We suggest that the mean ks of coccolith could be a potential proxy for the carbonate dissolution in the bottom water, especially in sites near or below the lyscocline.

Carbonate dissolution may also happen within the shallow sediment (Sulpis et al., 2021; Subhas et al., 2022). Based on our current dataset and using only the morphological variations, we cannot distinguish where the dissolution happens at the time of deposition in the sediment water interface, or post-burial in the first cms of the seafloor sediment. For the deep ocean deposits with lower sedimentary rates, such as the deepest parts of the SCS (Huang and Wang, 2006), the exposure time of particles to bottom water should be longer than that along the continental slope. Thus, we suggest that the major dissolution in the deep SCS happens on the sediment-water boundary instead of within pore water. Interestingly, the ks of coccolith in the surface sediment of the ECS are much lower, as low as 0.01 (Jin et al., 2019), than those in our study, which is higher than 0.04. However, the ks of coccolith during the laboratory dissolution experiment performed by Jin et al. (2019; Fig. 9A in that study) show the same range as our measurements. The ECS samples are from the continental shelf with high sedimentary rates and organic carbon content (Jin et al., 2019). In these settings, the coccoliths continuously dissolve after being buried within the first centimeters of the seafloor sediments in response to organic matter remineralization and CO_2 release, resulting in a ~30-50 % decrease in coccolith mass (Jin et al., 2019). Therefore, the sedimentary environment has to be individually evaluated to understand which process is controlling the dissolution of coccolithophores at the seafloor. More detailed work, such as in-situ pore water chemistry measurements, would be necessary to fully reveal the fate of coccolith dissolution in different burial scenarios (Holcová and Scheiner, 2022).

Among all the morphological parameters, we find the mean ks of coccolith is a more robust dissolution proxy compared to the other measured morphological parameters. Firstly, we observe a higher correlation coefficient between mean ks of coccolith and Ω_{Ca} compared with other morphological parameters. Secondly, although volume, mass, and thickness are also highly correlated with Ω_{Ca}, these morphological parameters vary more with the feature of different coccolithophores, including variations in coccolith circularity and cell sizes (Young and Ziveri, 2000; Bolton et al., 2016). Thirdly, the thickness is a morphological pattern sensitive to the upper ocean's preservation and surface ocean nutrients conditions during biomineralization (Table 2). Another important feature of ks is its high sensitivity to dissolution. As shown in Fig. 4, the ks of coccolith have already begun to decrease even though the water depths are only at ~2000 m, which is below the modern lysocline but above the CDD in the SCS (Wang et al., 1995; Luo et al., 2018). Finally, the dissolution effects on morphological attributes of mean ks agree

well with the laboratory dissolution experiment, in which each subsample's mean ks reflected different preservation stages (Fig. 4).

Despite a noticeable degree of uncertainty due to the mixing of life-cycle and post-mortem signals in the sedimentary record, similar findings of calcite dissolution modifying coccolith's morphology in waters at or below saturation suggest that the conclusions drawn from the present study are not unique to the SCS. In the Sub-Antarctic and Antarctic zone, dissolution signals affecting coccolithophores were manifested as a decrease in mass and distal shield length of *E. huxleyi* coccoliths preserved in surface sediments (Rigual-Hernández et al., 2020b; Vollmar et al., 2022). Based on this collective evidence, a key reasonable question could be, can the morphological variation of coccoliths be employed to trace their evolution safely, or instead be a good proxy for carbonate preservation?

5.3. Implications for interpreting the downcore history of coccolithophore morphology

On longer time scales, the morphological variations of coccoliths have been employed to trace coccolithophores evolutionary trends. Bolton et al. (2016) first measured the ks of Noëlaerhabdaceae in the last 15 million years. They found that the decrease of coccolith ks paralleled the reduction of atmospheric pCO_2 since the late Miocene and interpreted this as a decrease in biomineralization. More recent works by Beaufort et al. (2022) and Jin et al. (2022b) focused on the coccolithophore evolution over the last 2 million years by measuring coccolith mass, highlighting the role of seasonality and local environments in the evolution and production of Noëlaerhabdaceae. Similarly, Guitián et al. (2020) studied size trends across different regions between Oligocene to the Early Miocene, concluding that cell size distribution was controlled by multiple competing factors, with a strong selective pressure from CO_2 decline as a potential mechanism. This study examined dissolution by looking, among others, at the fragmentation and etching of coccoliths and found that temporal trends in lith size distributions were not significantly affected. This agrees with our observations since the mean length in SCS surface sediments does not correlate with any saturation state related parameter. However, Guitián et al. (2022), using a new calibration in the C-Calcita software that enables estimations of coccolith thickness up to 3.1 microns, found that elliptical ks (kse) was inversely correlated with the relative abundance of dissolution-resistant nannoliths. This was interpreted as a dissolution control on the elliptical shape factors in coccolithophores between Oligocene and Miocene, as it was found in our surface sediment samples. Therefore, we propose that for studies focusing on coccolithophore evolutionary histories, it would be safer to select a shallow

sediment core with low organic carbon content, high clay content, and always lying above the carbonate lysocline (Guitián et al., 2020).

One useful way to identify dissolution in these studies covering geological time scales could be plotting the σ/ks against ks. If an increase of σ/ks is detected in the sediment coccolith without any significant variations in coccolith assemblage or with an increase in dissolution-resistant species (Guitián et al., 2022), it should be interpreted as dissolution. Another way to determine separate evolutionary/ecological influences on ks variations could be to measure the ks of coccolith across a close spatial gradient which includes different depositional depths. Significant variations in the morphological attributes of the fossil coccolithophores would likely be caused by different saturation through time at different sites. Related to this last suggestion, coupling downcore morphological assessment in coccolithophores with other calcareous proxies measurements, such as size-normalized weight of planktic foraminiferal tests (Lohman, 1995; Broecker and Clark, 2001; Barker et al., 2002), which include recent advances in morphological analyses in large microfossils (Iwasaki et al., 2015; 2019), may provide an even more precise and safe quantitative estimates of past deep-carbonate chemistry parameters.

6. Summary

This study demonstrates, based on morphological attributes of *E. huxleyi* and *Gephyrocapsa* spp. (> 2 μm), that dissolution effects primarily affect the morphology of coccoliths preserved in the deep ocean. In the SCS surface sediments, bottom water Ω_{ca} saturation plays a major role in the variation of the coccoliths' ks shape factor, which has the potential, based on the current calibration, to quantitatively reconstruct past carbonate dissolution changes. Our laboratory-controlled dissolution results show that the mean ks decreased in response to increased amounts of corrosive solution. We propose the normalized ks variation to evaluate the degree of dissolution (light, strong, or no dissolution) occurring in the sedimentary record. A length-related dissolution pattern was also observed in the laboratory and surface sediments, with small coccoliths more prone to dissolution, increasing larger coccolith specimens and affecting the assemblage composition. As in the laboratory experiment, the coccolith's ks from surface sediments decreased with dissolution, and the σ/ks trajectory reflected different dissolution stages. However, the σ/ks in surface sediment showed a more complex response due to the natural variability of the surface sediment samples in terms of geographical differences in multiple environmental factors. These findings demonstrate that, despite the complementary of the carbonate system and ecological aspects, the coccoliths ks factor allied to σ/ks ratio has potential as a dissolution proxy to track changes in the seafloor carbonate saturation state. Although a stable proxy, the mean ks should be applied with caution,

particularly when applied to longer time scales, in which evolutionary trends might exert control on morphological attributes of fossil coccolithophores.

Author contributions

AG, HZ, RHN and IHA conceived and designed the study. AG and HZ conducted the lab work and sample analyses. AG, HZ and IHA performed the statistical analysis. AG, HZ and IHA wrote the manuscript with substantial contributions from all co-authors.

Competing interests

The authors declare that they have no conflict of interest.

Data availability

Research data is available as supplementary material and in the Zenodo (https://doi.org/10.5281/zenodo.7271441, Gerotto et al., 2022) and PANGAEA (https://doi.pangaea.de/10.1594/PANGAEA.954015 and https://doi.pangaea.de/10.1594/PANGAEA.954016, Gerotto et al., 2023a,b) data repositories.

Acknowledgments

This study was financed in part by the Coordenação de Aperfeiçoamento de Pessoal de Nível Superior - Brasil (CAPES) - Finance Code 001 to A.G. and the ETH Core and Swiss National Science Foundation (Award 200021_182070) funding to H. M. Stoll. Additional funding was provided by the National Natural Science Foundation of China (grants 42188102 and 41930536) to C.L. Thanks also to the International Ocean Discovery program for providing the sample used for the dissolution experiment.

References

Archer, D., Winguth, A., Lea, D., and Mahowald, N. What caused the glacial/interglacial atmospheric pCO_2 cycles? Rev. Geophys., 38(2), 159–189, https://doi.org/10.1029/1999RG000066, 2000.

Barker, S., and Elderfield, H. Foraminiferal calcification response to glacial-interglacial changes in atmospheric CO_2, Science, 297(5582), 833-836, https://doi.org/10.1126/science.1072815, 2002.

Båtvik, H., Heimdal, B. R., Fagerbakke, K. M., Green, J. C. Effects of unbalanced nutrient regime on coccolith morphology and size in *Emiliania huxleyi* (Prymnesiophyceae), Eur. J. Phycol., 32(2), 155–165, https://doi.org/10.1080/09670269710001737089, 1997.

566 Beaufort, L. Weight estimates of coccoliths using the optical properties (birefringence) of calcite,
567 Micropaleontology, 51(4), 289-297, https://doi.org/10.2113/gsmicropal.51.4.289,
568 2005.
569 Beaufort, L., Gally, Y., Suchéras-Marx, B., Ferrand, P., and Duboisset, J. A universal method for
570 measuring the thickness of microscopic calcite crystals, based on bidirectional circular
571 polarization, Biogeosciences, 18(3), 775-785, https://doi.org/10.5194/bg-18-775-2021,
572 2021.
573 Beaufort, L., Probert, I., De Garidel-Thoron, T., Bendif, E. M., Ruiz-Pino, D., Metzl, N., et al.
574 Sensitivity of coccolithophores to carbonate chemistry and ocean acidification, Nature,
575 476, 80–83, https://doi.org/10.1038/nature10295, 2011.
576 Beaufort, L., Probert, I., and Buchet, N. Effects of acidification and primary production on
577 coccolith weight: Implications for carbonate transfer from the surface to the deep
578 ocean, Geochem., Geophy., Geosy., 8(8), 1–18,
579 https://doi.org/10.1029/2006GC001493, 2007.
580 Beaufort, L., Bolton, C. T., Sarr, A. C., et al. Cyclic evolution of phytoplankton forced by changes
581 in tropical seasonality, Nature, 601, 79–84, https://doi.org/10.1038/s41586-021-04195-
582 7, 2022.
583 Bollmann, J. Weight approximation of coccoliths using a circular polarizer and interference
584 colour derived retardation estimates – (The CPR Method), Biogeosciences, 11, 1899-
585 1910, https://doi.org/10.5194/bg-11-1899-2014, 2014.
586 Bollmann, J., Herrle, J. O. Morphological variation of *Emiliania huxleyi* and sea surface salinity,
587 Earth Planet. Sc. Lett., 255(3-4), 273–288, https://doi.org/10.1016/j.epsl.2006.12.029,
588 2007.
589 Bolton, C. T., Hernández-Sánchez, M. T., Fuertes, M. Á., González-Lemos, S., Abrevaya, L.,
590 Mendez-Vicente, A., et al. Decrease in coccolithophore calcification and CO_2 since the
591 middle Miocene, Nat. Commun., 7, 10284, https://doi.org/10.1038/ncomms10284,
592 2016.
593 Bordiga, M., Bartol, M., Henderiks, J. Absolute nannofossil abundance estimates: Quantifying
594 the pros and cons of different techniques, Rev. de Micropaleontol., 58, 155-165,
595 https://doi:10.1016/j.revmic.2015.05.002, 2015.
596 Broecker, W. S., and Clark, E. Glacial-to-Holocene Redistribution of Carbonate Ion in the Deep
597 Sea, Science, 294(5549), 2152–2155, http://www.jstor.org/stable/3085356, 2001.
598 Broerse, A. T. C., Ziveri, P., and Honjo, S. Coccolithophore (-$CaCO_3$) flux in the Sea of Okhotsk:
599 Seasonality, settling and alteration processes, Mar. Micropaleontol., 39(1–4), 179–200,
600 https://doi.org/10.1016/S0377-8398(00)00020-7, 2000.

Buiteveld, H. A model for calculation of diffuse light attenuation (PAR) and Secchi depth, Neth. J. Aquat. Ecol., 29, 55–65, https://doi.org/10.1007/BF02061789, 1995.

Charalampopoulou, A., Poulton, A. J., Bakker, D. C. E., Lucas, M. I., Stinchcombe, M. C., Tyrrell, T. Environmental drivers of coccolithophore abundance and calcification across Drake Passage (Southern Ocean), Biogeosciences, 13, 5917–5935, https://doi.org/10.5194/bg-13-5917-2016, 2016.

Chen, C. T. A., Wang, S. L., Chou, W. C., and Sheu, D. D. Carbonate chemistry and projected future changes in pH and CaCO3 saturation state of the South China Sea, Mar. Chem., 101(3–4), 277–305, https://doi.org/10.1016/j.marchem.2006.01.007, 2006.

Chen, C. T. A., Wang, S. L., Wang, B. J., and Pai, S. C. Nutrient budgets for the South China sea basin, Mar. Chem., 75(4), 281–300, https://doi.org/10.1016/S0304-4203(01)00041-X, 2001.

Chen, Y. L. L. Spatial and seasonal variations of nitrate-based new production and primary production in the South China Sea, Deep-Sea Res. Pt. I, 52(2), 319–340, https://doi.org/10.1016/j.dsr.2004.11.001, 2005.

Chen, Y. L. L., Chen, H. Y., and Chung, C. W. Seasonal variability of coccolithophore abundance and assemblage in the northern South China Sea, Deep-Sea Res. Pt. II: Top. Stud. Oceanogr., 54(14–15), 1617–1633, https://doi.org/10.1016/j.dsr2.2007.05.005, 2007.

Chou, W. C., Sheu, D. D., Lee, B. S., Tseng, C. M., Chen, C. T. A., Wang, S. L., and Wong, G. T. F. Depth distributions of alkalinity, TCO_2 and δ^{13} $CTCO_2$ at SEATS time-series site in the northern South China Sea, Deep-Sea Res. Pt. II: Top. Stud. Oceanogr., 54(14–15), 1469–1485, https://doi.org/10.1016/j.dsr2.2007.05.002, 2007.

Conkright, M. E., Locarnini, R. A., Garcia, H. E., O'Brien, T. D., Boyer, T. P., Stephens, C., Antonov, J. I. World Ocean Atlas 2001: Objective Analyses, Data Statistics, and Figures, CD-ROM Documentation. National Oceanographic Data Center, Silver Spring, MD, 17 pp, 2002.

Emerson, S. R., and Archer, D. Calcium carbonate preservation in the ocean. Philos. Tr. R. Soc. S-A., 331(1616), 29–40, https://doi.org/10.1098/rsta.1990.0054, 1990.

Eppley, R. W., Rogers, J. N., and Mccarthy, J. J. Half-saturation constants for uptake of nitrate and ammonia, Liminol. Oceanogr., 14(6), 912–920, https://doi.org/10.4319/lo.1969.14.6.0912, 1969.

Feldmeijer, W., Metcalfe, B., Scussolini, P., and Arthur, K. The effect of chemical pretreatment of sediment upon foraminiferal-based proxies, Geochem., Geophy., Geosy., 14(10), 3996-4014, https://doi.org/10.1002/ggge.20233, 2013.

Fernando, A. G. S, Peleo-Alampay, A. M., Lucero, E. S., and Wiesner, M. G. Surface sediment distribution of *Florisphaera profunda* in the South China Sea: an effect of dissolution? J. Nannoplankton Res., 29(2), 102–07, 2007a.

Fernando, A. G. S., Peleo-Alampay, A. M., and Wiesner, M. G. Calcareous nannofossils in surface sediments of the eastern and western South China Sea, Mar. Micropaleontol., 66, 1–26, https://doi.org/10.1016/j.marmicro.2007.07.003, 2007b.

Flores, J. A., Marino, M., Sierro, F. J., Hodell, D. A., and Charles, C. D. Calcareous plankton dissolution pattern and coccolithophore assemblages during the last 600 kyr at ODP Site 1089 (Cape Basin, South Atlantic): Paleoceanographic implications. Palaeogeogr. Palaeocl., 196(3–4), 409–426, https://doi.org/10.1016/S0031-0182(03)00467-X, 2003.

Fuertes, M. Á., Flores, J. A., and Sierro, F. J. The use of circularly polarized light for biometry, identification and estimation of mass of coccoliths, Mar. Micropaleontol., 113, 44–55, https://doi.org/10.1016/j.marmicro.2014.08.007, 2014.

Gerotto, A., Zhang, H., Nagai, R. H., Stoll, H. M., Figueira, R. C. L., Chuanlian, L., Hernández-Almeida, I. Morphological measurements of coccoliths from surface samples of South China Sea, Zenodo [data set], https://doi.org/10.5281/zenodo.7271441, 2022.

Gerotto, A., Zhang, H., Nagai, R. H., Stoll, H. M., Figueira, R. C. L., Chuanlian, L., Hernández-Almeida, I. Morphological measurements of coccoliths from surface samples of R/V SONNE cruise SO95. PANGAEA, https://doi.pangaea.de/10.1594/PANGAEA.954015, 2023a.

Gerotto, A., Zhang, H., Nagai, R. H., Stoll, H. M., Figueira, R. C. L., Chuanlian, L., Hernández-Almeida, I. Coccolith dissolution experiment from one sample of ODP Hole 130-807A. PANGAEA, https://doi.pangaea.de/10.1594/PANGAEA.954016, 2023b.

González-Lemos, S., Guitián, J., Fuertes, M. Á., Flores, J. A., and Stoll, H. M. Technical note: An empirical method for absolute calibration of coccolith thickness, Biogeosciences, 15(4), 1079–1091, https://doi.org/10.5194/bg-15-1079-2018, 2018.

Goyet, C., Healy, R. J., and Ryan, J. P. Global distribution of total inorganic carbon and total alkalinity below the deepest winter mixed layer depths. ORNL/CDIAC-127, NDP-076. Carbon Dioxide Information Analysis Center, Oak Ridge National Laboratory, U.S. Department of Energy, Oak Ridge, Tennessee, 2000.

Guitián, J., Dunkley Jones, T., Hernández-Almeida, I., Löffel, T., and Stoll, H. M. Adaptations of coccolithophore size to selective pressures during the Oligocene to Early Miocene high CO2 world, Paleoceanogr. Paleoclimatology, 35(12), e2020PA003918, https://doi.org/10.1029/2020PA003918, 2020.

668 Guitián, J., Fuertes, M. Á., Flores, J. A., Hernández-Almeida, I., and Stoll, H. Variation in
669 calcification of Reticulofenestra coccoliths over the Oligocene-Early Miocene, Biogeosci.
670 Discuss., 1-17, https://doi.org/10.5194/bg-19-5007-2022, 2022.
671 Hammer, Ø., Harper, D. A. T., Ryan, P. D. PAST: Paleontological Statistics Software Package for
672 Education and Data Analysis, Palaeonto. Electron., 4(1), 1–9,
673 doi.org/10.1016/j.bcp.2008.05.025, 2001.
674 Hay, W. W. Carbonate fluxes and calcareous nannoplankton.
675 H. Thierstein, J. Young (Eds.), Coccolithophores: From Molecular Processes to Global
676 Impact, Springer, Berlin (2004), pp. 509-528, 2004.
677 Henderiks, J., and Pagani, M. Refining ancient carbon dioxide estimates: Significance of
678 coccolithophore cell size for alkenone-based pCO_2 records, Paleoceanography, 22(3), 1–
679 12, https://doi.org/10.1029/2006PA001399, 2007.
680 Hernández, A. S. R., Trull, T. W., Nodder, S. D., Flores, J. A., Bostock, H., Abrantes, F., et al.
681 Coccolithophore biodiversity controls carbonate export in the Southern Ocean,
682 Biogeosciences, 17(1), 245–263, https://doi.org/10.5194/bg-17-245-2020, 2020.
683 Holcová, K., and Scheiner, F. An experimental study on post-mortem dissolution and overgrowth
684 processes affecting coccolith assemblages: A rapid and complex process, Geobiology,
685 00, 1–17, https://doi.org/10.1111/gbi.12528, 2022.
686 Hönisch, B., Ridgwell, A., Schmidt, D. N., Thomas, E., Gibbs, S. J., Sluijs, A., et al. The geological
687 record of ocean acidification, Science, 335(6072), 1058–1063,
688 https://doi.org/10.1126/science.1208277, 2012.
689 Huang, W., and Wang, P. Sediment mass and distribution in the South China Sea since the
690 Oligocene. Sci. China Ser. D Earth Sci. 49, 1147–1155. https://doi:10.1007/s11430-006-
691 2019-4, 2006.
692 Iglesias-Rodriguez, M. D., Halloran, P. R., Rickaby, R. E. M., Hall, I. R., Colmenero-Hidalgo, E.,
693 Gittins, J. R., et al. Phytoplankton calcification in a high-CO_2 world, Science, 320(5874),
694 336–340, https://doi.org/10.1126/science.1154122, 2008.
695 IPCC: Climate Change and Land: an IPCC special report on climate change, desertification, land
696 degradation, sustainable land management, food security, and greenhouse gas fluxes in
697 terrestrial ecosystems [P.R. Shukla, J. Skea, E. Calvo Buendia, V. Masson-Delmotte, H.-
698 O. Pörtner, D. C. Roberts, P. Zhai, R. Slade, S. Connors, R. van Diemen, M. Ferrat, E.
699 Haughey, S. Luz, S. Neogi, M. Pathak, J. Petzold, J. Portugal Pereira, P. Vyas, E. Huntley,
700 K. Kissick, M. Belkacemi, J. Malley, (eds.)]. In press, 2019.

Iwasaki, S., Kimoto, K., Okazaki, Y., and Ikehara, M. Micro-CT scanning of tests of three planktic foraminiferal species to clarify dissolution process and progress, Geochem., Geophy., Geosy., 20(12), 6051-6065, https://doi.org/10.1029/2019GC008456, 2019.

Iwasaki, S., Kimoto, K., Sasaki, O., Kano, H., Honda, M. C., and Okazaki, Y. Observation of the dissolution process of *Globigerina bulloides* tests (planktic foraminifera) by X-ray microcomputed tomography, Paleoceanography, 30(4), 317-331, https://doi.org/10.1002/2014PA002639, 2015.

Johnsen, S. L., and Bollmann, J. Segmentation, retardation and mass approximation of birefringent particles on a standard light microscope, J. Microsc., 280, 30-50, https://doi.org/10.1111/jmi.12932, 2020.

Jin, X., Liu, C., Poulton, A. J., Dai, M., and Guo, X. Coccolithophore responses to environmental variability in the South China Sea: Species composition and calcite content, Biogeosciences, 13(16), 4843–4861, https://doi.org/10.5194/bg-13-4843-2016, 2016.

Jin, X., Liu, C., Xu, J., and Guo, X. Coccolithophore abundance, degree of calcification, and their contribution to particulate inorganic carbon in the South China Sea, J. Geophys. Res-Biogeo., 127(4), e2021JG006657, https://doi.org/10.1029/2021JG006657, 2022a.

Jin, X., Liu, C., and Zhang, H. Coccolith morphological and assemblage responses to dissolution in the recent sediments of the East China Sea, Mar. Micropaleontol., 152, 101709, https://doi.org/10.1016/j.marmicro.2018.09.001, 2019.

Jin, X., Ma, W., and Liu, C. Origin of the long-term increase in coccolith size and its implication for carbon cycle and climate over the past 2 Myr, Quaternary Sci. Rev., 290, 107642, https://doi.org/10.1016/j.quascirev.2022.107642, 2022b.

Le, J., and Shackleton, N. J. Carbonate dissolution fluctuations in the western equatorial Pacific during the late Quaternary, Paleoceanography, 7, 21–42, https://doi.org/10.1029/91PA02854, 1992.

Libes, S. M. An Introduction to Marine Biogeochemistry, 2nd ed. Burlington, MA: Academic Press Noone, K., Sumaila, R.; Diaz R.J. (eds) 2009. Valuing the Oceans, Stockholm Environmental Institute, 2009.

Lin, J., Lee, Z., Ondrusek, M., and Du, K. Remote sensing of normalized diffuse attenuation coefficient of downwelling irradiance, J. Geophys. Res-Oceans, 121(9), 6717-6730, https://doi.org/10.1002/2016JC011895, 2016.

Liu, J., Xiang, R., Chen, M., Chen, Z., Yan, W., and Liu, F. Influence of the Kuroshio current intrusion on depositional environment in the Northern South China Sea: Evidence from surface sediment records, Mar. Geol., 285(1–4), 59–68, https://doi.org/10.1016/j.margeo.2011.05.010, 2011.

Lohman, G. P. A model for variation in the chemistry of planktonic foraminifera due to secondary calcification and selective dissolution, Paleoceanogr. Paleoclimatology, 10(3), 445-457, https://doi.org/10.1029/95PA00059, 1995.

Luo, Y., Kienast, M., and Boudreau, B. P. Invariance of the carbonate chemistry of the South China Sea from the glacial period to the Holocene and its implications to the Pacific Ocean carbonate system, Earth Planet. Sci. Lett., 492, 112–120, https://doi.org/10.1016/j.epsl.2018.04.005, 2018.

Marsaglia, K., Milliken, K., Leckie, R., M., Tentori, D., Doran, L. IODP Smear Slide Digital Reference for Sediment Analysis of Marine Mud. Part 2: Methodology and Atlas of Biogenic Components. IODP Technical Note 2, doi:10.14379/iodp.tn.2.2015, 2015.

Murtugudde, R., Beauchamp, J., McClain, C. R., Lewis, M., and Busalacchi, A. Effects of penetrative radiation on the upper tropical ocean circulation, J. Climate, 15(5), 470-486, https://doi.org/10.1175/1520-0442(2002)015<0470:EOPROT>2.0.CO;2, 2002.

Paasche, E. Roles of nitrogen and phosphorus in coccolith formation in *Emiliania huxleyi* (Prymnesiophyceae), Eur. J. Phycol., 33(1), 33-42, https://doi.org/10.1080/09670269810001736513, 1998.

Pälike, H., Lyle, M. W., Nishi, H., Raffi, I., Ridgwell, A., Gamage, K., et al. A Cenozoic record of the equatorial Pacific carbonate compensation depth, Nature, 488(7413), 609–614, https://doi.org/10.1038/nature11360, 2012.

Pälike, H., Norris, R. D., Herrle, J. O., Wilson, P. A., Helen, K., Lear, C. H., et al. The heartbeat of the Oligocene climate system, Science, 314(5807), 1894–1898, https://www.jstor.org/stable/20035092, 2006.

Pierrot, D., Lewis, E., and Wallace, D. W. R. MS Excel Program Developed for CO_2 System Calculations - version 2.1. ORNL/CDIAC-105a. Carbon Dioxide Information Analysis Center, Oak Ridge National Laboratory, U.S. Department of Energy, Oak Ridge, Tennessee, https://doi.org/10.3334/CDIAC/otg.CO2SYS_XLS_CDIAC105a, 2012.

Pinxian, W., Qiubao, M., Yunhua, B., and Wenke, F. Planktonic foraminifera in the continental slope of the northern South China Sea during the last 130,000 years and their paleo-oceanographic implications, Acta Geol. Sin-Engl., 60(3), 1–11, https://doi.org/10.1111/j.1755-6724.1986.mp60003001.x, 1986.

Qu, T., Girton, J. B., and Whitehead, J. A. Deepwater overflow through Luzon Strait, J. Geophys. Res., 111(C1), C01002, https://doi.org/10.1029/2005JC003139, 2006.

Qu, T., Song, Y. T., and Yamagata, T. An introduction to the South China Sea throughflow: Its dynamics, variability, and application for climate, Dynam. Atmos. Oceans, 47(1–3), 3–14, https://doi.org/10.1016/j.dynatmoce.2008.05.001, 2009.

Rae, J. W. B., Zhang, Y. G., Liu, X., Foster, G. L., Stoll, H. M., and Whiteford, R. D. M. Atmospheric CO_2 over the past 66 million years from marine archives, Annu. Rev. Earth Pl. Sc., 49, 609–641, https://doi.org/10.1146/annurev-earth-082420-063026, 2021.

Raven, J. A., and Crawfurd, K. Environmental controls on coccolithophore calcification. Mar. Ecol. Prog. Ser., 470, 137–166. http://www.jstor.org/stable/24876210, 2012.

Rhodes, L. L., Peake, B. M., MacKenzie, A. L., and Marwick, S. Coccolithophores *Gephyrocapsa oceanica* and *Emiliania huxleyi* (Prymnesiophyceae = Haptophyceae) in New Zealand's coastal waters: Characteristics of blooms and growth in laboratory culture, N. Z. J. Mar. Freshwater Res., 29:3, 345-357, https://doi.org/10.1080/00288330.1995.9516669, 1995.

Rickaby, R. E. M., Bard, E., Sonzogni, C., Rostek, F., Beaufort, L., Barker, S., et al. Coccolith chemistry reveals secular variations in the global ocean carbon cycle? Earth Planet. Sci. Lett., 253(1–2), 83–95, https://doi.org/10.1016/j.epsl.2006.10.016, 2007.

Ridgwell, A., and Zeebe, R. E. The role of the global carbonate cycle in the regulation and evolution of the Earth system, Earth Planet. Sci. Lett., 234(3–4), 299–315, https://doi.org/10.1016/j.epsl.2005.03.006, 2005.

Riebesell, U., Zondervan, I., Rost, B., Tortell, P. D, Zeebe, R. E., and Morel, F. M. M. Reduced calcification of marine plankton in response to increased atmospheric CO_2, Nature, 407, 364–367, https://doi.org/10.1038/35030078, 2000.

Rigual-Hernández, A. S., Sánchez-Santos, J. M., Eriksen, R., Moy, A. D., Sierro, F. J., Flores, J. A., et al. Limited variability in the phytoplankton *Emiliania huxleyi* since the pre-industrial era in the Subantarctic Southern Ocean. Anthropocene, 31, 100254, https://doi.org/10.1016/j.ancene.2020.100254, 2020b.

Rigual-Hernández, A. S., Trull, T. W., Nodder, S. D., Flores, J. A., Bostock, H., Abrantes, F., Eriksen, R.S., Sierro, F. J., Davies, D. M., Ballegeer, A.-M., Fuertes, M. A., and Northcote, L. C. Coccolithophore biodiversity controls carbonate export in the Southern Ocean, Biogeosciences, 17, 245–263, https://doi.org/10.5194/bg-17-245-2020, 2020a.

Roth, P. H., and Berger, W. H. Distribution and dissolution of coccoliths in the South and Central Pacific. Sliter, W. V., Be,´ A. W. H., Berger, W. H. (Eds.), Dissolution of Deep-Sea Carbonates, Cushman Foundation Foraminiferal Research, Spec. Publ., N. 13, pp. 87-113, 1975.

Roth, P. H., and Coulbourn, W. T. Floral and solution patterns of coccoliths in surface sediments of the North Pacific. Mar. Micropaleontol., 7(1), 1-52, https://doi.org/10.1016/0377-8398(82)90014-7, 1982.

Sarmiento, J. L., Gruber, N. Ocean Biogeochemical dynamics. Princeton, NJ, Woodstock: Princeton University Press. 528 pp, 2006.

Schlitzer, R. Ocean data View. Available at:<htt://odv.awi.de>, 2019.

Stoll, H. M., Ziveri, P. Separation of monospecific and restricted coccolith assemblages from sediments using differential settling velocity, Mar. Micropaleontol., 46(1–2), 209-221, https://doi.org/10.1016/S0377-8398(02)00040-3, 2002.

Su, X., Liu, C., and Beaufort, L. Late Quaternary coccolith weight variations in the northern South China Sea and their environmental controls, Mar. Micropaleontol., 154, 101798, https://doi.org/10.1016/j.marmicro.2019.101798, 2020.

Subhas, A. V., Dong, S., Naviaux, J. D., Rollins, N. E., Ziveri, P., Gray, W., et al. Shallow calcium carbonate cycling in the North Pacific Ocean, Global Biogeochem. Cy., 36(5), 1–22, https://doi.org/10.1029/2022GB007388, 2022.

Sulpis, O., Boudreau, B. P., Mucci, A., Jenkins, C., Trossman, D. S., Arbic, B. K., and Key, R. M. Current $CaCO_3$ dissolution at the seafloor caused by anthropogenic CO_2, P. Natl. Acad. Sci. USA, 115(46), 11700–11705, https://doi.org/10.1073/pnas.1804250115, 2018.

Sulpis, O., Jeansson E., Dinauer A., Lauvset, S. K., and Middelburg, J. J. Calcium carbonate dissolution patterns in the ocean, Nat. Geosci., 14(6), 423–428, http://dx.doi.org/10.1038/s41561-021-00743-y, 2021.

Thunell, R. C., Qingmin, M., Calvert, S. E., and Pedersen, T. F. Glacial-Holocene biogenic sedimentation patterns in the South China Sea: Productivity variations and surface water pCO_2, Paleoceanography, 7(2), 143–162, https://doi.org/10.1029/92PA00278, 1992.

Tian, J., Huang, E., and Pak, D. K. East Asian winter monsoon variability over the last glacial cycle: Insights from a latitudinal sea-surface temperature gradient across the South China Sea, Palaeogeogr. Palaeocl., 292(1–2), 319–324, https://doi.org/10.1016/j.palaeo.2010.04.005, 2010.

USGCRP. Climate Science Special Report: Fourth National Climate Assessment, Volume I [Wuebbles, D. J., Fahey, D. W., Hibbard, K. A., Dokken, D. J., Stewart, B. C., and Maycock, T. K. (eds.)]. U.S. Global Change Research Program, Washington, DC, USA, 470 pp., 2017.

Vollmar, N. M., Baumann, K. H., Saavedra-Pellitero, M., and Hernández-Almeida, I. Distribution of coccoliths in surface sediments across the Drake Passage and calcification of *Emiliania huxleyi* morphotypes, Biogeosciences, 19(3), 585–612, https://doi.org/10.5194/bg-19-585-2022, 2022.

838 Wan, S., and Jian, Z. Deep water exchanges between the South China Sea and the Pacific since
839 the last glacial period, Paleoceanography, 29(12), 1162–1178,
840 https://doi.org/10.1002/2013PA002578, 2014.
841 Wan, S., Jian, Z., and Dang, H. Deep Hhydrography of the South China Sea and deep water
842 circulation in the Pacific since the Last Glacial Maximum, Geochem., Geophy., Geosy.,
843 19(5), 1447–1463, https://doi.org/10.1029/2017GC007377, 2018.
844 Wan, S., Jian, Z., Gong, X., Dang, H., Wu, J., and Qiao, P. Deep water [CO_3^{2-}] and circulation in
845 the South China Sea over the last glacial cycle, Quat. Sci. Rev., 243, 106499,
846 https://doi.org/10.1016/j.quascirev.2020.106499, 2020.
847 Wang, N., Huang, B.-Q., and Li, H. Deep-water carbonate dissolution in the northern South China
848 Sea during Marine Isotope Stage 3, J. Palaeogeogr., 5(1), 100–107,
849 https://doi.org/10.1016/j.jop.2015.11.004, 2016.
850 Wang, P., Li, Q., and Dai, M. The South China Sea Deep: Introduction, Deep-Sea Res. Pt. II: Top.
851 Stud. Oceanogr, 122, 1-5, https://doi.org/10.1016/j.dsr2.2015.11.004, 2015.
852 Wang, P., Wang, L., Bian, Y., and Jian, Z. Late Quaternary paleoceanography of the South China
853 Sea: surface circulation and carbonate cycles, Mar. Geol., 127(1–4), 145–165,
854 https://doi.org/10.1016/0025-3227(95)00008-M, 1995.
855 Wang, P. X., and Li, Q. Y. The South China Sea: Paleoceanography and Sedimentology. Springer,
856 Berlin, Heidelberg, New York, p. 506, 2009.
857 Young, J. R., and Ziveri, P. Calculation of coccolith volume and its use in calibration of carbonate
858 flux estimates, Deep-Sea Res. Pt. II: Top. Stud. Oceanogr., 47(9–11), 1679–1700,
859 https://doi.org/10.1016/S0967-0645(00)00003-5, 2000.
860 Yu, J., and Elderfield, H. Benthic foraminiferal B/Ca ratios reflect deep water carbonate
861 saturation state, Earth Planet. Sci. Lett., 258(1–2), 73–86,
862 https://doi.org/10.1016/j.epsl.2007.03.025, 2007.
863 Yu, J., Menviel, L., Jin, Z. D., Thornalley, D. J. R., S. Barker, S., Marino, G., et al. Sequestration of
864 carbon in the deep Atlantic during the last glaciation, Nat. Geosci., 9, 319-324,
865 https://doi.org/10.1038/ngeo2657, 2016.
866 Zachos, J. C., Röhl, U., Schellenberg, S. A., Sluijs, A., Hodell, D. A., Kelly, D. C., et al. Paleoclimate:
867 Rapid acidification of the ocean during the Paleocene-Eocene thermal maximum,
868 Science, 308(5728), 1611–1615, https://doi.org/10.1126/science.1109004, 2005.
869 Zhang, H., Liu, C., Jin, X., Shi, J., Zhao, S., and Jian, Z. Dynamics of primary productivity in the
870 northern South China Sea over the past 24,000 years, Geochem., Geophy., Geosy.,
871 17(12), 4878–4891, https://doi.org/10.1002/2016GC006602, 2016.

872